SCIENCE CHINA Materials ARTICLES

mater.scichina.com link.springer.com Published online 18 May 2020 | https://doi.org/10.1007/s40843-020-1335-x

High-performance polyamide nanofiltration membrane with arch-bridge structure on a highly hydrated cellulose nanofiber support

Xiangxiu Teng[1,2,3,4], Wangxi Fang[1], Yuanzhe Liang[5], Shihong Lin[5], Hongzhen Lin[1], Shasha Liu[6], Zhenyi Wang[1], Yuzhang Zhu[1*] and Jian Jin[1,2*]

ABSTRACT **Nanofiltration (NF) membranes with outstanding performance are highly demanded for more efficient desalination and wastewater treatment. However, improving water permeance while maintaining high solute rejection by using the current membrane fabrication techniques remains a challenge. Herein, polyamide (PA) NF membrane with arch-bridge structure is successfully prepared *via* interfacial polymerization (IP) on a composite support membrane of salt-reinforced hydrophilic bacterial cellulose nanofibers (BCNs) nanofilm/polytetrafluoroethylene (BCNs/PTFE). The strong hydration of BCNs promotes Marangoni convection along water/organic solvent interface during the IP process, which creates extra area for interfacial reaction and produces a thin PA active layer with arch-bridge structures. These arch-bridge structures endow the resulting PA active layer with substantial larger active area for water permeation. Consequently, the PA NF membrane exhibits exceptional desalination performance with a permeance up to 42.5 L m^{-2} h^{-1} bar^{-1} and a rejection of Na_2SO_4 as high as 99.1%, yielding an overall desalination performance better than almost all of the state-of-the-art NF membranes reported so far in terms of perm-selectivity.**

Keywords: nanofiltration membrane, crumpled structure, cellulose nanofibers, interfacial polymerization, desalination

INTRODUCTION

Water scarcity has evolved to be a global challenge due to climate change and economic growth [1–3]. Sustainable fresh water supply *via* seawater/brackish desalination is actively explored as a technological solution to the water scarcity challenge [4,5]. In comparison with other desalination technologies, reverse osmosis (RO) and nanofiltration (NF) membrane-based technologies are energy-efficient and technologically mature [4,6,7]. With a high rejection of multivalent ions and organic molecules with molecular weight cutoff (MWCO) higher than 200 Da [8–10], NF is an ideal technology for low-energy, high-throughput desalination applications. Enhancing the water permeance of an NF membrane is highly desirable for reducing the energy consumption or/and the required membrane area. However, dramatic improvement of water permeance without compromising the salt rejection remains a technical challenge due to the intrinsic tradeoff between permeability and selectivity [11,12].

The state-of-the-art NF membranes are thin film composite (TFC) PA membranes formed *via* interfacial polymerization (IP) on a porous support [13–19]. Even though the PA layer is typically only dozens of nanometer thick, its properties dominate the perm-selectivity of the TFC-PA membrane. Therefore, engineering the properties of the PA layer is of paramount importance to enhancing membrane performance and has thus been the focus of many recent studies [20–26]. Typical strategies of tailoring the properties of the PA active layer for improving permeance include making thinner PA layer and incorporating hydrophilic nanomaterials into the layer to reduce water transport resistance [17,27–30], which have been extensively investigated. Alternatively, increasing the

[1] i-Lab, Suzhou Institute of Nano-Tech and Nano-Bionics, Chinese Academy of Sciences, Suzhou 215123, China
[2] School of Physical Science and Technology, Shanghai Tech University, Shanghai 200031, China
[3] Shanghai Institute of Ceramics, Chinese Academy of Sciences, Shanghai 200050, China
[4] University of Chinese Academy of Sciences, Beijing 100049, China
[5] Department of Civil and Environmental Engineering, Vanderbilt University, Nashville, TN 37235-1831, United States
[6] College of Chemistry and Chemical Engineering, Qilu Normal University, Jinan 250200, China
* Corresponding authors (emails: yzzhu2011@sinano.ac.cn (Zhu Y); jjin2009@sinano.ac.cn (Jin J))

specific surface area of PA active layer is another highly effective route to enhance the permeance without sacrificing selectivity. Two classic examples following this design strategy include the recent work by Wang *et al.* [31] who proposed a nanoparticles-templated IP process to construct PA active layer with crumpled structures, and that by Tan *et al.* [32] who designed a Turing-type PA active layer by tuning the diffusion of the piperazine (PIP) monomers in IP process. Both studies proved that the enhanced specific surface area resulting from the engineered surface morphology provided more effective area for water permeation, which resulted in dramatic improvement in perm-selectivity.

During the IP process for fabricating TFC-PA NF or/and RO membranes, the interfacial reaction between the amine monomer and trimesoyl chloride (TMC) is a rapid polymerization reaction releasing a large amount of heat (i.e., strongly exothermic). The released heat will cause a steep rise of local temperature and induce strong fluid convection (i.e., Marangoni convection) and interfacial turbulence at the interface. This convection is thought to be responsible for the formation of the distinct crumpled structure of PA layer in TFC-PA RO membranes as often observed [19,28,33–36]. In comparison with the IP process for TFC-PA RO membranes, the reaction between amine monomers (PIP) and TMC is not as vigorous as for TFC-PA NF membranes, thereby inducing a lower temperature gradient along the liquid/liquid interface in IP. In addition, the TFC-PA NF membranes are commonly prepared on commercial ultrafiltration (UF) or microfiltration (MF) membranes. These UF/MF membranes typically have poor water wettability and low surface porosity, which often result in discrete patches for interfacial reaction as water is prone to be confined in the pores of these porous supports instead of fully-spreading on their surfaces. The mass transfer driven by Marangoni convection at the interface is thus impeded and PA active layers with discrete spots were often observed in TFC-PA NF membranes [37–39]. We hypothesize that enhancing the surface water wettability of porous support facilitates the formation of a continuous hydration layer, which could result in a continuous and homogeneous water/hexane interface for the IP process. This continuous and homogeneous water/hexane interface could in turn promote the lateral mass transfer driven by Marangoni convection and the formation of PA active layer with larger specific surface area. By strengthening the Marangoni convection during IP process, we fabricate TFC-PA NF membrane with a special arch-bridge structure using a salt-reinforced hydrophilic bacterial cellulose nanofiber (BCN) nanofilm pre-deposited onto a polytetrafluoroethylene (PTFE) MF membrane (BCNs/PTFE) as a composite porous support. Due to the abundance of hydroxyl and carboxyl groups on the surface of BCNs, the BCNs/PTFE composite support membrane is highly hydrophilic. Sodium chloride (NaCl) was also added into the PIP aqueous solution to further enhance the hydration of the BCN nanofilm, giving rise to a thick and continuous water layer on BCNs/PTFE as shown in Scheme 1a.

Once the TMC organic solution was brought into contact with the salt-containing PIP solution on the surface of BCNs/PTFE composite support, a continuous and homogeneous water/hexane interface formed. The formation of such a continuous interface facilitates the IP reaction throughout the entire interface and induces strong Marangoni convection across a larger length scale, which results in a PA active layer with relatively large, arch-bridge rough structure (Scheme 1b). In comparison, conventional IP process conducted on a poorly-wetted UF support results in a PA active layer with small spotted structures due to restricted lateral mass transfer along the water/hexane interaction and suppressed Marangoni convection (Scheme 1c).

EXPERIMENTAL SECTION

Materials

Hydrophilic PTFE MF membrane (0.45 μm) was purchased from Hangzhou Annuo Filter Material Co. Ltd (China). Polyethersulfone (PES) UF (NADIR UH050, MWCO 50,000 Da) membrane was purchased from Microdyn-Nadir. Bacterial cellulose was provided by Hainan Yide Food Co. Ltd (Haikou, China). SWCNTs powder (diameter < 2 nm, length > 5 μm, purity 95%) was purchased from XFNANO (Nanjing, China). TMC, PIP, sodium periodate ($NaIO_4$), and sodium hypochlorite (NaClO) were all purchased from Aladdin Chemical Co. Ltd (Shanghai, China). Other chemicals were all obtained from Sinopharm Co. Ltd. and used as received without further purification.

Characterization and instruments

The infrared spectra were collected by using a Fourier transform infrared (FT-IR) spectrometer (Nicolet 6700). Scanning electron microscopy (SEM) images were obtained from a cold field emission scanning electron microscope (Hitachi S4800) under deceleration mode. Transmission electron microscopy (TEM) images were acquired from a transmission electron microscope (Hi-

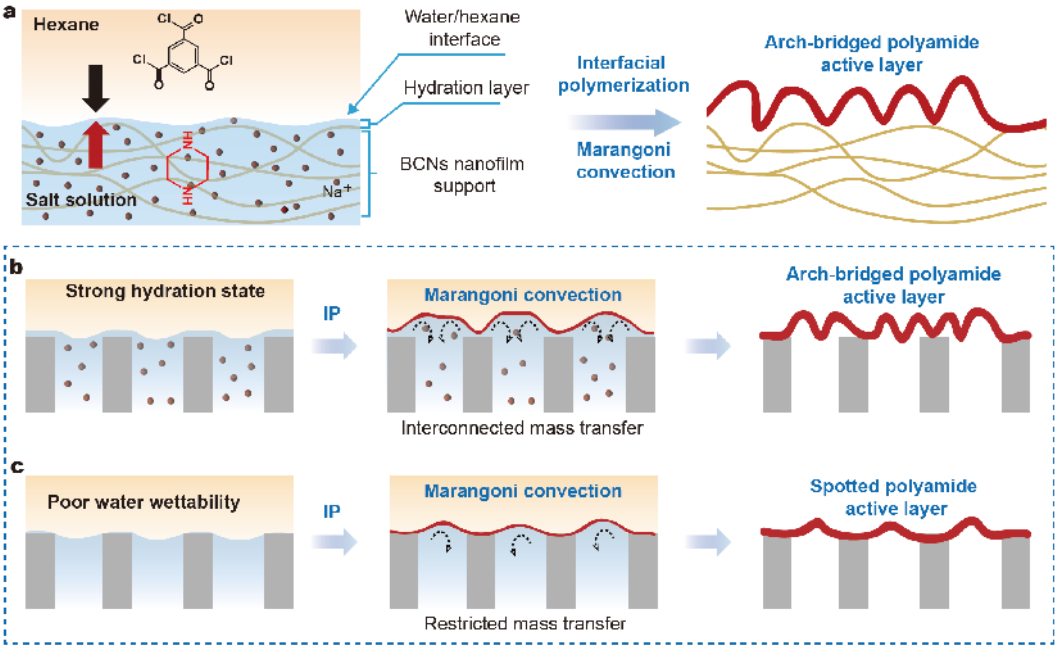

Scheme 1 Fabrication of arch-bridge TFC PA NF membrane. (a) Schematic of IP of PA on NaCl-reinforced hydrophilic BCN nanofilm. A schematic demonstrating the formation of PA active layer with arch-bridge structure on a support with good water wettability (b) and with spotted structure on a support with poor water wettability (c).

tachi HT7700). The TEM samples were prepared by embeding a small piece of PA NF membrane in resin, and then cutting the resin by ultramicrotome (Leica EM UC7) to obtain ultra-thin slices with thickness of 30–60 nm. Atomic force microscopy (AFM) images were obtained by a Bruker Dimension Icon atomic force microscope in tapping mode. Surface Zeta potential was measured on a solid surface analysis (Anton Paar Surpass 3). X-ray photoelectron spectroscopy (XPS) spectra were collected by an X-ray photoelectron spectrometer (Thermo Fisher Scientific ESCALAB 250Xi). Dynamic water contact angle (CA) was measured on a Data-Physics OCA 20 with 3 μL water droplet as probe. The concentration of polyethylene glycol (PEG) aqueous solution was determined by total organic carbon (TOC) analysis (OI Analytical Aurora Model 1030). The sum frequency generation (SFG) spectrometer was set up by EKSPLA with a copropa gating configuration. The visible laser pulse at 532 nm and IR pulses around 3000–3800 cm^{-1} are < 30 ps at 50 Hz. The incident angle is 60° for the visible beam, and 55° for the IR beam. The energy of the visible and IR beams is generally less than 200 mJ and no photo-damage was observed during the measurements. The polarization combination for the IR, visible and SFG signal beams was typically ssp (s-polarized sum frequency output, s-polarized visible input, and p-polarized IR input) during the experiment. The polymer film of interest was placed in a Teflon cell, which was lidded with a half-cylinder CaF_2 prism as an optical window. The cell was filled with pure water or salt solutions of different concentrations. The distance between the sample plane and the prism bottom was tunable so that the thickness of the sandwiched liquid layer could be well controlled. The assembled cell was put on a *x*-*y*-*z* sample stage, and the leveling and *z*-position of the sample plane were carefully adjusted to make sure the SFG signal was collected from the polymer film/salt solution interface.

Fabrication of bacterial cellulose nanofiber dispersion

The bacterial cellulose nanofibers were prepared as follows: bacterial cellulose bulk was firstly boiled in the NaOH solution (0.1 mol L^{-1}) for 1 h. Then $NaIO_4$ solution (0.05 mol L^{-1}) and NaClO solution (4 mmol L^{-1}) were used successively to oxide the cellulose as shown in reactions (S1) and (S2) (see the Supplementary information). After being washed with pure water for 3–5 times, the oxidized bacterial cellulose was added into Milli-Q water and sonicated for 1.5 h. The dispersion was then centrifuged at 10,000 rpm for 30 min and the supernatant was collected. The achieved BCN dispersion was stored at 4°C for further use. The concentration of the BCN dispersion is around 1.6 mg mL^{-1}.

Fabrication of TFC PA NF membrane

The BCNs/PTFE composite membrane was prepared by filtering the BCN dispersion onto a hydrophilic PTFE MF membrane (0.45 μm). The IP then conducted on the surface of BCNs/PTFE composite support according to the following steps: 0.25 g of PIP with a certain amount of NaCl (from 0.5 to 2 g) was dissolved in 100 mL of pure water to produce 0.25 wt% PIP aqueous solution. The amine group concentration in the PIP aqueous solution was around 58 mmol L^{-1}. 0.5 g of TMC was dissolved in 100 mL of anhydrous *n*-hexane to produce a TMC hexane solution, where the acyl chloride group concentration was around 56.5 mmol L^{-1}. The BCNs/PTFE composite support was tapped on a glass plate and then immersed in PIP aqueous solution for 1 min. After being taken out from the PIP aqueous solution, the glass plate was drained vertically for 3–5 min to remove the extra solution. Then, TMC solution was introduced on the surface of BCNs/PTFE composite membrane for 1 min. The prepared TFC NF membrane was washed with fresh hexane to remove unreacted TMC and dried under 60°C for 30 min and then stored in water for further use.

Membrane performance test

The desalination performance of as-prepared PA NF membranes was examined by a lab-scale cross-flow filtration apparatus in which a circular cell with an effective area of 7.1 cm^2 was used to fix the membrane. The applied transmembrane pressure was fixed at 2 bar and the concentrations of all feed salt solutions were 1000 ppm if there is no special description. To ensure steady state, the NF membranes were pre-pressurized by pure water at 4 bar for 2 h. The permeates were collected for measuring the rejection and corresponding permeance after running for 30 min. The permeance of PA NF membrane was calculated by using the following equation:

$$\text{Permeance} = \frac{\Delta w}{\rho A \Delta t \cdot \Delta P},$$

where Δw is the weight of collected permeate during filtration time Δt, A is the efficient separation area of 7.1 cm^2, ρ is the density of permeate and considered as 1 g mL^{-1}, ΔP is the applied transmembrane pressure for filtration experiment.

The rejection was calculated as follows:

$$R = \left(1 - \frac{C_p}{C_f}\right) \times 100\%,$$

where C_p and C_f represent the concentrations of permeate and feed solution, respectively, which were determined by detecting their conductivities.

Molecular dynamic simulation

A molecular nanofilm with size of 7.0 nm × 4.5 nm × 3.0 nm was constructed, where chemical structures of the molecules were same as functional groups on the surface of BCNs (as shown in the reaction (S2) in Supplementary information). Then, a pure water layer and a water layer containing 1 wt% NaCl with a thickness of 3.0 nm was added on the *z*-axis of the nanometer membrane, respectively. Molecular dynamic (MD) simulations were then performed using the GROMACS software package (version 4.5.4). The Gromos 54a7 force field was adopted for calculating the interatomic interactions. The force field parameters for this simulation are listed in Table S1. Each of the simulation systems was initialized by minimizing the energies of the initial configurations using the steepest descent method. Following the minimization, a 20 ns MD simulation under canonical ensemble (NVT) was carried out for each system, with a time step of 1 fs. In all simulations, the temperature was kept constant at 298 K by the Berendsen thermostat algorithm. Bond lengths were constrained using the LINCS algorithm and periodic boundary conditions were applied in all directions. Short-range nonbonded interactions were cut off at 1.2 nm, with long-range electrostatics calculated using the particle mesh Ewald method. Energy fluctuation and mean square displacement of water were used to evaluate whether the system equilibrated. Trajectories were stored every 1 ps.

The binding affinity of water molecules on the BCN nanofilm surface was reflected by the potential of mean force (PMF), calculated by the pair distribution function $g(r)$ of the nanofilm and water through the equation $E(r) = -k_B T \ln g(r)$, where k_B is Boltzmann's constant and T is the simulation temperature. Taking the NaCl reinforced BCN nanofilm as an example, the following conclusions can be made. i) The contact minimum (CM) in energy profile is at about 0.29 nm, corresponding to the direct contact between water and BCN nanofilm surface. ii) The second minimum is at a distance of 0.46 nm, which corresponds to the solvent-separated minimum (SSM). Both CM and SSM determine the binding affinity of water to the nanofilm surface. iii) The CM and SSM are separated by a desolvation barrier (BS) that must be overcome for transitions between the two minima. The calculated PMF tends to be zero with the increasing distance between the polymer surface and water.

RESULTS AND DISCCUSION

Characterization of arch-bridge PA NF membrane

Bacterial cellulose bulk was used as the raw material for

preparing the BCN nanofilm. Bacterial cellulose has a typical network structure composed of abundant fine nanofibers with a diameter around 10 nm as shown in Fig. S1. Due to rich hydroxyl groups on the surface of nanofibers, bacterial cellulose bulk is highly hydrophilic and can retain a large amount of water within the network (Fig. 1a). The bacterial cellulose was oxidized by $NaIO_4$ and subsequently reduced by NaClO in order to prepare a translucent aqueous dispersion of BCNs (Fig. 1b). During this process, the six-membered oxygen heterocycles of sugar were opened and the original hydroxyl groups were transformed into carboxyl groups (see reactions (S1) and (S2) in Supplementary information). The chemical composition of BCNs was further confirmed by FT-IR spectrometer and XPS as shown in Figs S2 and S3. AFM image shows the well dispersed nanofibers with diameters around 8–10 nm based on the height profile (Fig. 1c, d). These ultrafine nanofibers were then deposited onto the surface of a commercial PTFE MF membrane (Fig. S4) *via* vacuum filtration to form a BCN nanofilm. The top-view SEM image of BCN nanofilm shows a smooth and uniformly porous network structure (Fig. 1e). The thicknesses of BCN nanofilm is about 400 nm based on the cross-section SEM image (Fig. 1f). This BCN nanofilm could be peeled off from the PTFE MF membrane. A free-standing BCN nanofilm dyed with Direct Red 80 floating on water (Fig. 1g) could maintain its structural integrity even when it is lifted from water (Fig. 1h). The free-standing BCN nanofilm without staining is colorless and transparent (Fig. S5). These results indicate that the BCNs indeed interconnect with each other and form an integral film.

The surface water wettability of BCN nanofilm was evaluated by monitoring the change of water CA with respect to time. As shown in Fig. 2a, the water CA of the BCN nanofilm is initially 68.8° and decreases to 28.6° within 30 s. As for the aqueous solution containing 1 wt% NaCl, the CA of BCN nanofilm is initially 58.3° and decreases to 22.3° within 30 s, indicating that NaCl can enhance the hydrophilicity of BCN nanofilm. The permeance variation of BCN nanofilm as a function of time is shown in Fig. 2b. The BCN nanofilm shows higher permeance when the aqueous solution containing 1 wt% NaCl passes through it. This result also indicates the reinforced hydrophilicity of BCN nanofilm by NaCl.

TFC-PA NF membranes were fabricated *via* IP using BCNs/PTFE composite membrane as the support and PIP aqueous solution with different concentrations of NaCl. SEM image of the TFC-PA NF membrane prepared from PIP aqueous solution without addition of NaCl shows a rough surface with irregular microstructures (Fig. 3a). Discrete spotted structures are clearly observed using AFM (Fig. 3b). In the case of the TFC-PA NF membrane prepared from PIP aqueous solution with NaCl, interconnected stripped structures are clearly observed using both SEM (Fig. 3d) and AFM (Fig. 3e). The two mem-

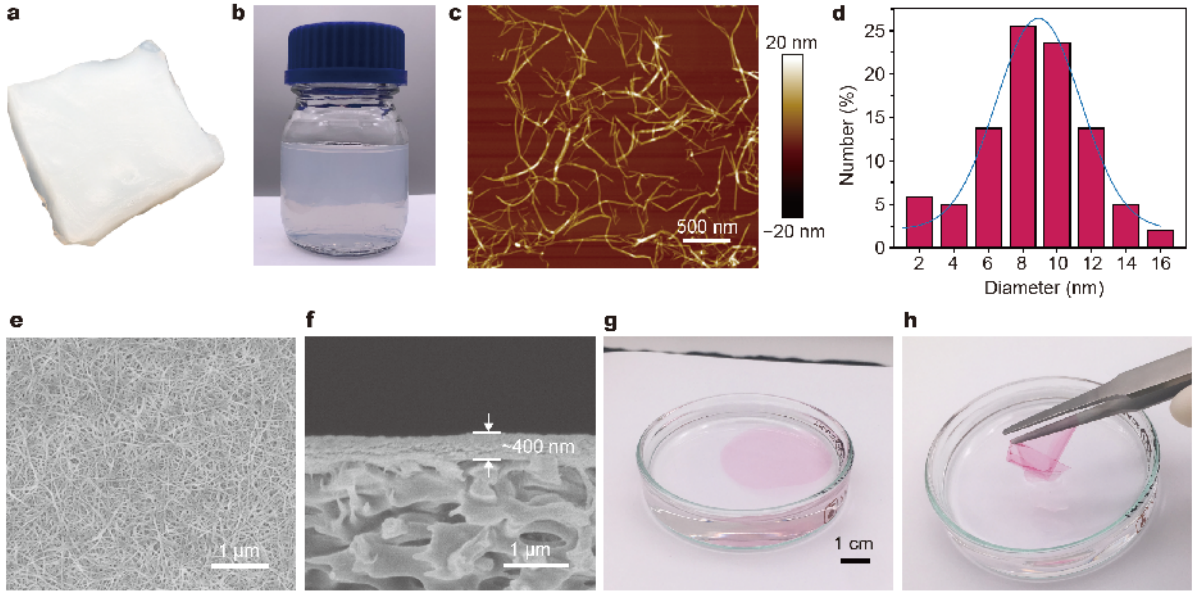

Figure 1 Characterization of BCNs and BCN nanofilm. (a, b) Photographs of bacterial cellulose bulk and BCN dispersion, respectively. (c, d) AFM image of BCNs and corresponding statistic distribution of BCN diameters. (e, f) Top view and cross-sectional SEM images of BCN nanofilm deposited on PTFE MF membrane. (g, h) Photographs of free-standing BCN nanofilm dyed by Direct Red 80.

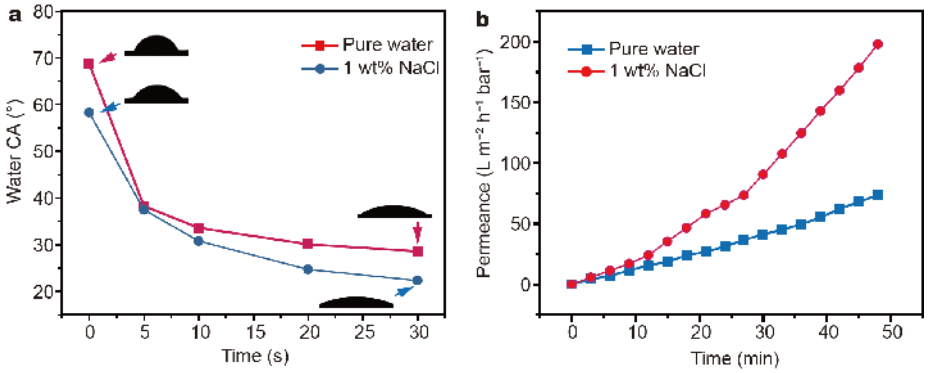

Figure 2 Effect of NaCl on the surface wettability and permeance of BCN nanofilm. (a) Surface wettability of the BCN nanofilm to pure water and water containing 1 wt% NaCl. (b) Permeance variation of the BCN nanofilm as a function of filtration time using pure water and 1 wt% NaCl aqueous solution as feed, respectively. Applied pressure is 1 bar.

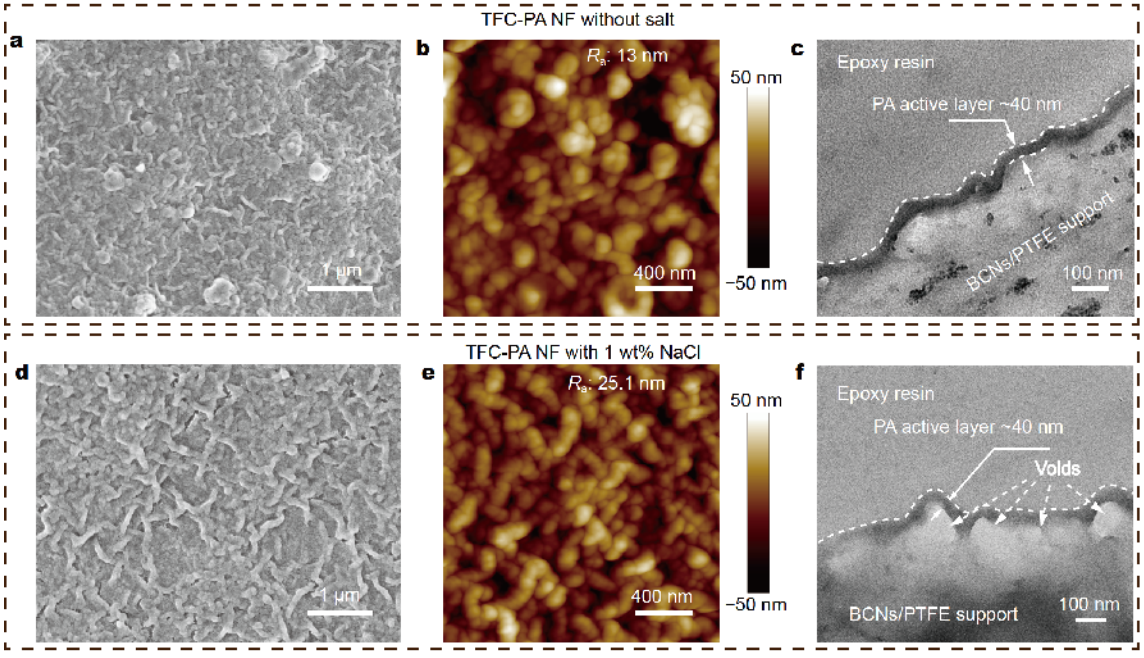

Figure 3 Structure characterization of TFC-PA NF membranes. (a) Top view SEM image, (b) AFM image, and (c) cross-sectional TEM image of the NF membrane prepared in PIP aqueous solution without addition of salt. (d) Top view SEM image, (e) AFM image, and (f) TEM image of the cross-sectional membrane prepared in PIP aqueous solution with the addition of 1 wt% NaCl.

branes both have a thin PA active layer with a uniform thickness (~40 nm) as shown in Fig. 3c and f, but differ in their ways of connecting to the underlying support. In the case of TFC-PA NF membrane prepared from PIP aqueous solution without addition of NaCl, the upper thin PA layer in dark color is tightly bound to the underlying support (e.g., BCN nanofilm) in light color (Fig. 3c), without any void space in-between. In contrast, large arch-bridge structures between the PA layer and BCN nanofilm are observed in the case of TFC-PA NF membrane prepared by using PIP aqueous solution with NaCl (Fig. 3f).

Effect of salt on the membrane performance

The impact of the NaCl concentration in PIP aqueous solution on the perm-selectivity of the TFC-PA NF membranes was investigated with 1000 ppm Na_2SO_4 as the feed solution. Increasing the NaCl concentration in aqueous PIP solution from 0 to 1 wt% enhances the permeances of TFC-PA NF membranes from 18.5 to

42.5 L m^{-2} h^{-1} bar^{-1} while maintaining the rejections to Na_2SO_4 above 98.5% (Fig. 4a). The increase of permeance is mainly attributable to the formation of the arch-bridge structure on the PA active layer that provides more effective area for water permeation (Fig. S6). Further increasing the NaCl concentration in PIP aqueous solution to 2 wt% continued to improve the permeance to 45.5 L m^{-2} h^{-1} bar^{-1} but at the cost of reducing the rejection of Na_2SO_4 to 94.6 %.

The improvement of perm-selectivity by salt addition into the PIP solution is not only effective with NaCl but also with other monovalent salts such as LiCl and KCl (Fig. S7). In all cases, more than two-fold enhancements of the permeance were measured without any observable compromise in Na_2SO_4 rejection (Fig. S7). Stripped structures are also observed in PA active layer (Fig. S8), indicating the similar impact of LiCl and KCl on the morphology of the PA active layers to that of NaCl. Notably, the addition of salts does not change the pore size distribution of the active layer as all the resulting membranes have the same MWCO of around 300 Da based on the rejection of PEG molecules with different molecular weights (Fig. 4b), which corresponds to a mean pore size of 0.36–0.38 nm. Additionally, XPS survey spectra of TFC-PA NF membrane prepared with and without additive of NaCl in PIP aqueous solution confirm no Na element (centered at 1070.8 eV) in the PA active layer (Fig. S9). These results reveal that the sole effect of adding monovalent salts in the IP process was to increase the specific surface area by inducing the formation of the arch-bridge structures.

To further evaluate the desalination performance of the TFC-PA NF membrane prepared with NaCl addition, we measured the membrane performance (permeance and rejection) with different feed solutions containing a single salt species of Na_2SO_4, $MgSO_4$, $MgCl_2$ and NaCl, re-

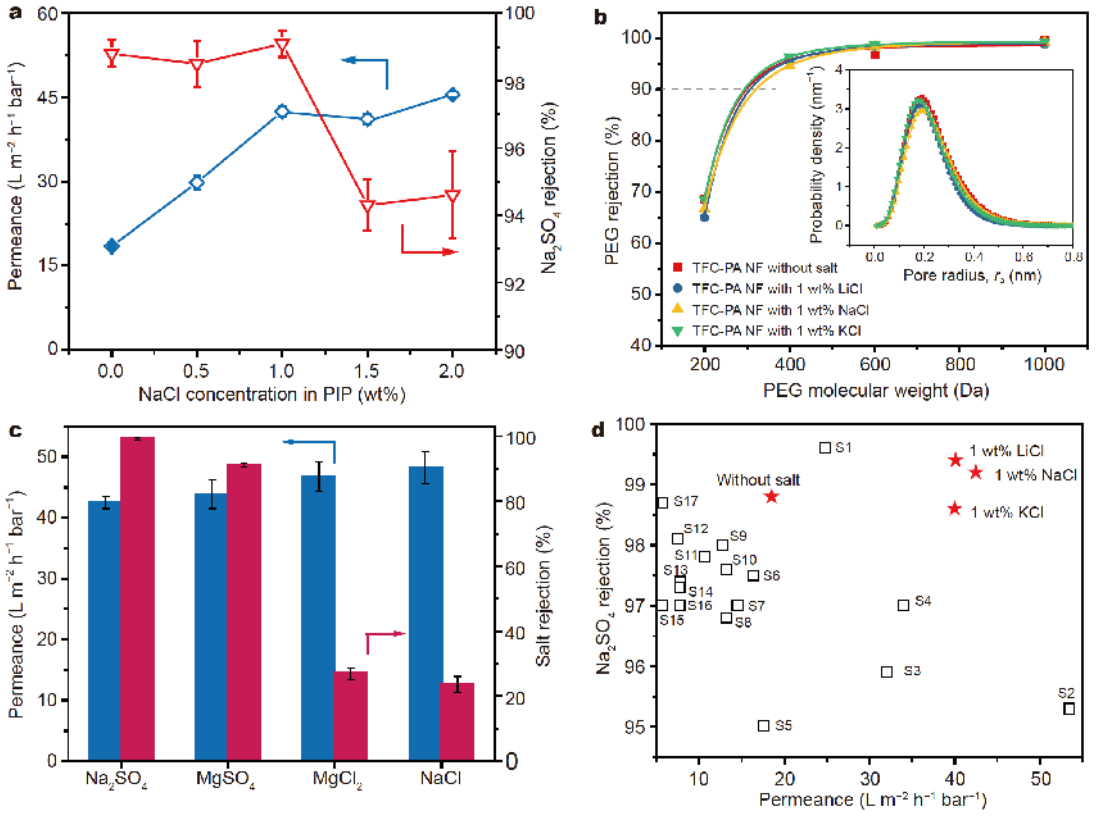

Figure 4 Desalination performance of TFC-PA NF membranes. (a) Variation of permeance and rejection of TFC-PA NF membrane as a function of NaCl concentration in PIP aqueous solution. (b) Rejection curves of the TFC-PA NF membranes prepared with the addition of 1 wt% NaCl, KCl and LiCl in PIP aqueous solution, respectively, to PEG with different molecular weights and corresponding pore size distributions (inset). (c) Permeance and corresponding rejection of the membrane prepared with the addition of 1 wt% NaCl in PIP aqueous solution to various salts as feed solutions (the concentrations of these feeds are all 1000 ppm). (d) Summary of the desalination performance of the state-of-the-art NF membranes reported previously and the membranes obtained in this work while using Na_2SO_4 solution as feed. The literatures cited in Fig. 4d (Ref. S1–S17) are listed in Supplementary information.

spectively (Fig. 4c). The membrane shows high rejection up to 99.1% and 91% for Na_2SO_4 and $MgSO_4$, respectively, with their corresponding permeances being 42.5 and 43.9 L m^{-2} h^{-1} bar^{-1}, respectively. In comparison, the rejections for $MgCl_2$ and NaCl are 27% and 23.6%, respectively, with the corresponding permeance being 46.7 and 48.2 L m^{-2} h^{-1} bar^{-1}, respectively. Similar membrane performance is also obtained with PA membranes prepared with 1 wt% LiCl and 1 wt% KCl in PIP aqueous solution (Figs S10, S11). In comparison with the desalination performance of TFC-PA NF membrane prepared without slat in PIP aqueous solution, the involvement of monovalent slat in PIP aqueous solution only improve the permeance without any change on the rejection behavior of NF membrane (Fig. S12).

The stability of the PA NF membrane was examined by monitoring the variation of permeance and rejection in prolonged cross-flow filtration with 1000 ppm Na_2SO_4 solution as the feed water under an applied pressure of 2 bar. The permeance and solute rejection remained stable throughout the filtration experiment with an area-specific permeate volume up to 660 mL cm^{-2} (Fig. S13). The stability of the PA NF membrane under applied pressure was also confirmed by the linear relationship between the permeate flux and applied pressure when the applied pressure increased from 2 to 8 bar (Fig. S14).

The performance of the PA NF membrane with arch-bridge structure is compared with the performance of the state-of-the-art NF membranes reported in literature (Fig. 4d and Supplementary Ref. s1–s17). The trade-off between permeance and solute rejection is particularly salient at high salt rejection regime where a slight increase of rejection is often achieved at the cost of a serious reduction of permeance. The membranes fabricated in this work by using the BCN support with the addition of monovalent salt exhibit exceptional permeance (> 40 L m^{-2} h^{-1} bar^{-1}) with outstanding Na_2SO_4 rejection (>98.3%). The overall desalination performance of our membranes surpasses almost all other NF membranes reported in literature.

Mechanism analysis of salt effect

The major improvement in perm-selectivity is attributable to the higher specific surface area as a consequence of the formation of the arch-bridge structure. We ascribe the formation of this special structure to the enhanced Marangoni convection that takes place on the surface of strongly hydrated BCN nanofilm during IP process. To investigate the impact of NaCl on the hydration state of BCN nanofilm, we used SFG vibrational spectroscopy to detect the water structure on BCN nanofilm surface with and without NaCl. SFG vibrational spectroscopy is a surface-sensitive spectroscopy for detecting molecular structure at various interfaces, especially air/solid and liquid/solid interfaces. BCN nanofilms were prewetted by either pure water or water containing NaCl with different concentrations and respective SFG spectra were collected (Fig. 5a). No signals are detected in the SFG vibrational spectra when the BCN nanofilm is dried or prewetted with pure water (Fig. 5b). In comparison, a broad peak at around 3200 cm^{-1} appears when the BCN nanofilms are prewetted by NaCl solutions. This peak corresponds to the O–H stretching vibration of water. In SFG spectra, the appearance of O–H stretching usually indicates the formation of strong hydrogen bond of water at the interface [40–42]. The intensity of SFG signal is correlated to the order of surface molecules at the interface. Stronger signal indicates higher order of the surface-bound molecules. With the increase of NaCl concentration from 0.5 to 2 wt%, the intensity of O–H stretching vibration increases and shifts to lower wavenumber, which suggests that the presence of NaCl promotes the hydration ability of water in the system. This is because that there is a strong electrostatic interaction between Na^+ ion and water molecules. Since Na^+ ions uniformly fill in the whole network of BCN nanofilm, a thicker hydration layer could be formed on the surface of BCN nanofilm. Molecular dynamics (MD) simulations were used to further understand the effect of NaCl on the hydration ability of BCN nanofilm. A BCN nanofilm with a size of 7.0 nm × 4.5 nm × 3.0 nm was constructed first and a 3.0 nm thick water layer containing 1 wt% NaCl was then added normal to the BCN nanofilm (see detail description in Supplementary information). In the control experiment, a 3.0 nm thick water layer containing no NaCl was added along the normal of the BCN nanofilm with the same size. After equilibrium dynamic simulations were performed for 20 ns, Na^+ ions (signed as blue spheres) were introduced into the network of the BCN nanofilm and simultaneously a thin water layer (water molecules are signed as yellow spheres) formed above its surface (Fig. 5c). Structure analysis performed by MD simulation indicates that the Na^+ ions uniformly distributed around BCNs and water molecules in the form of a thin water layer surround the out layer of Na^+ ions through forming hydrogen bond (Fig. 5d). To explore the intrinsic binding affinity of water to the surface of NaCl-reinforced hydrophilic BCN nanofilm, the PMF between BCNs and water molecules was calculated. The corresponding energy profiles are illustrated in Fig. 5e, in which the peaks

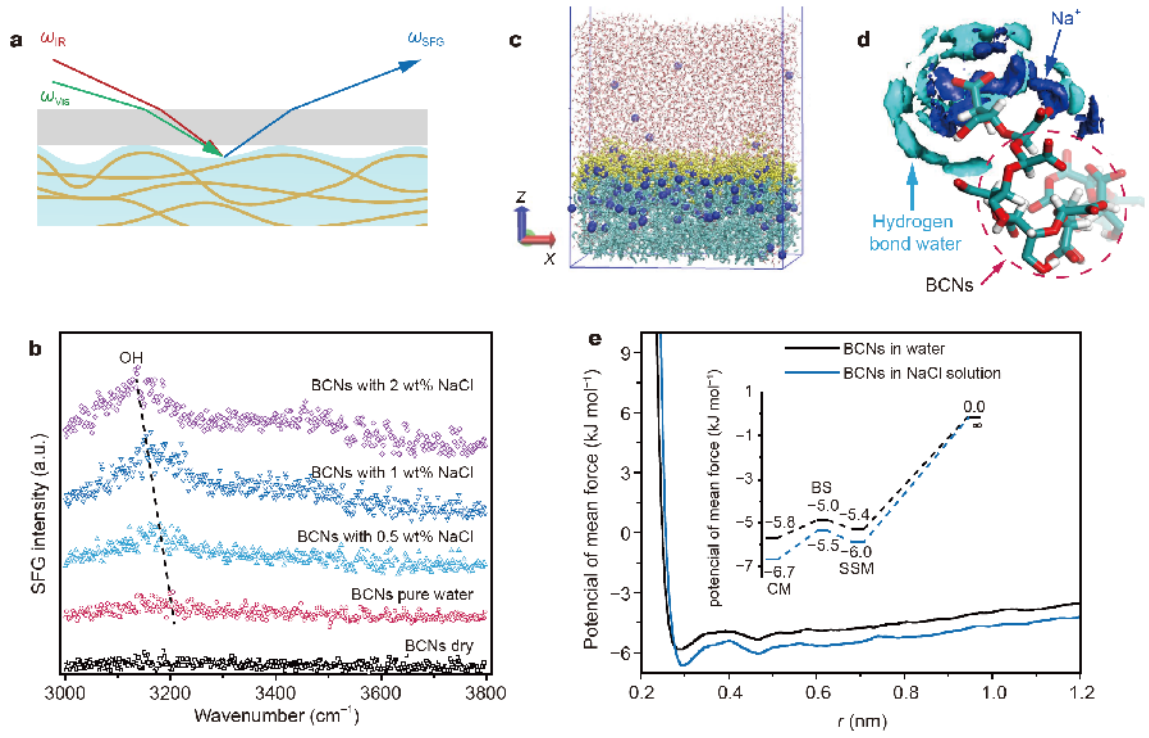

Figure 5 Characterization of the hydration state of BCN nanofilm. (a) Experimental scheme showing the test of SFG vibrational spectroscopy on BCN nanofilm. (b) SFG spectra of the BCN nanofilm in air, prewetted by pure water, and water containing NaCl with concentrations of 0.5 wt%, 1 wt%, and 2 wt%. (c) Snapshot of the simulation system composed by BCN nanofilm (signed as green), water molecules (signed as yellow spheres) and Na^+ ions (signed as blue spheres) after 20 ns simulation. (d) Enlarged MD simulated distribution of water molecules and Na^+ ions around BCNs. (e) PMF between the BCN nanofilm and water with and without NaCl.

and valleys in the profiles determine the binding affinity of water to the surface of BCNs. The dehydration energy was calculated to be 1.20 kJ mol^{-1} in the presence of NaCl and 0.80 kJ mol^{-1} without NaCl. This result proves that the presence of NaCl enhances the hydration ability in the system of water molecules and BCNs and facilitates the formation of stable hydration layer on the surface of BCN nanofilm.

In general, the support membranes used for fabricating TFC-NF membranes are commercial UF membranes, such as PES, polysulfone (PSF) and polyacrylonitrile (PAN). These support membranes are with poor water-wettability and low surface porosity, which often result in discrete patches for interfacial reaction as water is prone to be confined in the pores of these porous supports instead of fully-spreading on their surfaces. The mass transfer driven by Marangoni convection at the whole interface is thus impeded and the PA active layers with discrete spots are often observed in common TFC-PA NF membranes as shown in Scheme 1c. If the support membrane is with good water-wettability, for example superhydrophilic, then the support membrane surface will be loaded by a continuous water layer and present a continuous and homogeneous water/hexane interface as shown in Scheme 1b. The formation of such a continuous interface facilitates the mass transfer throughout the entire interface and induces enhanced Marangoni convection crossing to a larger length scale laterally. As a result, the PA active layer with crumpled rough structure is generated.

In this work, superhydrophilic BCN nanofilm deposited onto PTFE MF membrane was used as support membrane for preparing TFC-PA NF membrane *via* IP. Although BCN nanofilm is superhydrophilic, it behaves a strong water hydrogel to lock water on or in it through hydrogen bond interaction, giving rise to greatly reduced movability of the water layer and resulting in a rigid water/hexane interface. It therefore suppresses the Marangoni convection. NaCl has strong hydration ability. When adding NaCl in water, Na^+ ions will uniformly fill in the whole network of BCN nanofilm. Besides the strong hydration ability of NaCl itself, it can provide a charge shielding effect to weaken the hydrogen bond interaction between water and BCN nanofilm [43–45]. A

thicker and continuous water layer but with higher movability thus could form across the surface of BCN nanofilm confirmed by the permeance variation as a function of time as shown in Fig. 2b.

To further confirm the correlation between Marangoni convection and the arch-bridge structure, two control experiments have been done: (i) the IP process was carried out at low temperature of 4°C; (ii) the IP process was conducted by using low concentration of PIP and TMC (0.25 and 0.5 mg mL^{-1}, respectively, which were one tenth of those used in the manuscript). The SEM images of the two resulting membranes both show smooth surface and no obvious rough or crumpled structures are observed (Fig. S15). Since Marangoni convection is mainly caused by the local gradient of temperature or the concentration of reactive agents at the interface, these results confirm that the formation of the arch-bridge structure on the PA layer is attributed to Marangoni convection.

CONCLUSIONS

In summary, we report in this work the fabrication of TFC-PA NF membranes with a special arch-bridge morphology. The PA active layer with such an arch-bridge morphology was formed *via* enhanced Marangoni convection during the IP process where a salt-reinforced hydrophilic BCN nanofilm coated PTFE MF membrane was used as support. The arc-bridge structure increases the specific surface area of the NF membrane and creates more effective area for water permeation, yielding exceptional NF performance with a permeance up to 42.5 L m^{-2} h^{-1} bar^{-1} and a rejection of Na_2SO_4 up to 99.1%. The addition of salt doubles the permeance without compromising salt rejection, resulting in NF membranes outperforming almost all other NF membranes reported so far. This work provides a new insight to engineer the active layer morphology to transcend the current permittivity-selectivity tradeoff.

Received 1 April 2020; accepted 4 April 2020; published online 18 May 2020

1 Gleick PH. Global freshwater resources: soft-path solutions for the 21st century. Science, 2003, 302: 1524–1528
2 Mekonnen MM, Hoekstra AY. Four billion people facing severe water scarcity. Sci Adv, 2016, 2: e1500323
3 Vörösmarty CJ, Green P, Salisbury J, *et al.* Global water resources: vulnerability from climate change and population growth. Science, 2000, 289: 284–288
4 Elimelech M; Elimelech M, Phillip WA. The future of seawater desalination: energy, technology, and the environment. Science, 2011, 333: 712–717
5 Porada S, Zhao R, van der Wal A, *et al.* Review on the science and technology of water desalination by capacitive deionization. Prog Mater Sci, 2013, 58: 1388–1442
6 Greenlee LF, Lawler DF, Freeman BD, *et al.* Reverse osmosis desalination: Water sources, technology, and today's challenges. Water Res, 2009, 43: 2317–2348
7 Werber JR, Osuji CO, Elimelech M. Materials for next-generation desalination and water purification membranes. Nat Rev Mater, 2016, 1: 16018
8 Paul M, Jons SD. Chemistry and fabrication of polymeric nanofiltration membranes: A review. Polymer, 2016, 103: 417–456
9 Mohammad AW, Teow YH, Ang WL, *et al.* Nanofiltration membranes review: Recent advances and future prospects. Desalination, 2015, 356: 226–254
10 Zhou D, Zhu L, Fu Y, *et al.* Development of lower cost seawater desalination processes using nanofiltration technologies—A review. Desalination, 2015, 376: 109–116
11 Park HB, Kamcev J, Robeson LM, *et al.* Maximizing the right stuff: The trade-off between membrane permeability and selectivity. Science, 2017, 356: eaab0530
12 Geise GM, Park HB, Sagle AC, *et al.* Water permeability and water/salt selectivity tradeoff in polymers for desalination. J Membrane Sci, 2011, 369: 130–138
13 Hilal N, Al-Zoubi H, Darwish NA, *et al.* A comprehensive review of nanofiltration membranes: Treatment, pretreatment, modelling, and atomic force microscopy. Desalination, 2004, 170: 281–308
14 Sorribas S, Gorgojo P, Téllez C, *et al.* High flux thin film nanocomposite membranes based on metal–organic frameworks for organic solvent nanofiltration. J Am Chem Soc, 2013, 135: 15201–15208
15 Yoon K, Hsiao BS, Chu B. High flux nanofiltration membranes based on interfacially polymerized polyamide barrier layer on polyacrylonitrile nanofibrous scaffolds. J Membrane Sci, 2009, 326: 484–492
16 Choi W, Gu JE, Park SH, *et al.* Tailor-made polyamide membranes for water desalination. ACS Nano, 2015, 9: 345–355
17 Wang JJ, Yang HC, Wu MB, *et al.* Nanofiltration membranes with cellulose nanocrystals as an interlayer for unprecedented performance. J Mater Chem A, 2017, 5: 16289–16295
18 Bui NN, McCutcheon JR. Hydrophilic nanofibers as new supports for thin film composite membranes for engineered osmosis. Environ Sci Technol, 2013, 47: 1761–1769
19 Inukai S, Cruz-Silva R, Ortiz-Medina J, *et al.* High-performance multi-functional reverse osmosis membranes obtained by carbon nanotube·polyamide nanocomposite. Sci Rep, 2015, 5: 13562
20 Zhang Y, Su Y, Peng J, *et al.* Composite nanofiltration membranes prepared by interfacial polymerization with natural material tannic acid and trimesoyl chloride. J Membrane Sci, 2013, 429: 235–242
21 Wang C, Li Z, Chen J, *et al.* Covalent organic framework modified polyamide nanofiltration membrane with enhanced performance for desalination. J Membrane Sci, 2017, 523: 273–281
22 Zhou Z, Hu Y, Boo C, *et al.* High-performance thin-film composite membrane with an ultrathin spray-coated carbon nanotube interlayer. Environ Sci Technol Lett, 2018, 5: 243–248
23 Qian H, Zheng J, Zhang S. Preparation of microporous polyamide networks for carbon dioxide capture and nanofiltration. Polymer, 2013, 54: 557–564
24 An QF, Sun WD, Zhao Q, *et al.* Study on a novel nanofiltration membrane prepared by interfacial polymerization with zwitterionic amine monomers. J Membrane Sci, 2013, 431: 171–179
25 Li Y, He G, Wang S, *et al.* Recent advances in the fabrication of

advanced composite membranes. J Mater Chem A, 2013, 1: 10058–10077
26 Wang H, Zhang Q, Zhang S. Positively charged nanofiltration membrane formed by interfacial polymerization of 3,3′,5,5′-biphenyl tetraacyl chloride and piperazine on a poly(acrylonitrile) (PAN) support. J Membrane Sci, 2011, 378: 243–249
27 Zhu Y, Xie W, Gao S, *et al.* Single-walled carbon nanotube film supported nanofiltration membrane with a nearly 10 nm thick polyamide selective layer for high-flux and high-rejection desalination. Small, 2016, 12: 5034–5041
28 Karan S, Jiang Z, Livingston AG. Sub-10 nm polyamide nanofilms with ultrafast solvent transport for molecular separation. Science, 2015, 348: 1347–1351
29 Jeong BH, Hoek EMV, Yan Y, *et al.* Interfacial polymerization of thin film nanocomposites: a new concept for reverse osmosis membranes. J Membrane Sci, 2007, 294: 1–7
30 Ma H, Burger C, Hsiao BS, *et al.* Highly permeable polymer membranes containing directed channels for water purification. ACS Macro Lett, 2012, 1: 723–726
31 Wang Z, Wang Z, Lin S, *et al.* Nanoparticle-templated nanofiltration membranes for ultrahigh performance desalination. Nat Commun, 2018, 9: 2004
32 Tan Z, Chen S, Peng X, *et al.* Polyamide membranes with nanoscale Turing structures for water purification. Science, 2018, 360: 518–521
33 Li X, Wang KY, Helmer B, *et al.* Thin-film composite membranes and formation mechanism of thin-film layers on hydrophilic cellulose acetate propionate substrates for forward osmosis processes. Ind Eng Chem Res, 2012, 51: 10039–10050
34 Yin J, Kim ES, Yang J, *et al.* Fabrication of a novel thin-film nanocomposite (TFN) membrane containing MCM-41 silica nanoparticles (NPs) for water purification. J Membrane Sci, 2012, 423-424: 238–246
35 Chae HR, Lee J, Lee CH, *et al.* Graphene oxide-embedded thin-film composite reverse osmosis membrane with high flux, anti-biofouling, and chlorine resistance. J Membrane Sci, 2015, 483: 128–135
36 Ghosh AK, Hoek EMV. Impacts of support membrane structure and chemistry on polyamide–polysulfone interfacial composite membranes. J Membrane Sci, 2009, 336: 140–148
37 Chen Y, Liu F, Wang Y, *et al.* A tight nanofiltration membrane with multi-charged nanofilms for high rejection to concentrated salts. J Membrane Sci, 2017, 537: 407–415
38 Li L, Zhang S, Zhang X. Preparation and characterization of poly(piperazineamide) composite nanofiltration membrane by interfacial polymerization of 3,3′,5,5′-biphenyl tetraacyl chloride and piperazine. J Membrane Sci, 2009, 335: 133–139
39 Shen J, Yu C, Ruan H, *et al.* Preparation and characterization of thin-film nanocomposite membranes embedded with poly(methyl methacrylate) hydrophobic modified multiwalled carbon nanotubes by interfacial polymerization. J Membrane Sci, 2013, 442: 18–26
40 Leng C, Sun S, Zhang K, *et al.* Molecular level studies on interfacial hydration of zwitterionic and other antifouling polymers *in situ*. Acta Biomater, 2016, 40: 6–15
41 Leng C, Hung HC, Sieggreen OA, *et al.* Probing the surface hydration of nonfouling zwitterionic and poly(ethylene glycol) materials with isotopic dilution spectroscopy. J Phys Chem C, 2015, 119: 8775–8780
42 Nagasawa D, Azuma T, Noguchi H, *et al.* Role of interfacial water in protein adsorption onto polymer brushes as studied by SFG spectroscopy and QCM. J Phys Chem C, 2015, 119: 17193–17201
43 Chiu HC, Lin YF, Hung SH. Equilibrium swelling of copolymerized acrylic acid−methacrylated dextran networks: Effects of pH and neutral salt. Macromolecules, 2002, 35: 5235–5242
44 Liu H, Zhen M, Wu R. Ionic-strength- and pH-responsive poly[acrylamide-co-(maleic acid)] hydrogel nanofibers. Macromol Chem Phys, 2007, 208: 874–880
45 de Groot GW, Santonicola MG, Sugihara K, *et al.* Switching transport through nanopores with pH-responsive polymer brushes for controlled ion permeability. ACS Appl Mater Interfaces, 2013, 5: 1400–1407

Acknowledgements This work was supported by the National Natural Science Funds for Distinguished Young Scholar (51625306), the Key Project of the National Natural Science Foundation of China (21433012), the National Natural Science Foundation of China (51603229, 21406258), and the State Key Laboratory of Separation Membranes and Membrane Processes (Tianjin Polytechnic University, No. M1-201801). Funding support from the CAS Pioneer Hundred Talents Program is grateful appreciated as well.

Author contributions Zhu Y and Jin J designed the experiments and developed the theory; Teng X performed the experiments; Lin H performed the measurement of SFG; Liu S contributed to the MD analysis; Teng X, Liang Y, Wang Z, Fang W and Zhu Y performed the data analysis; Teng X and Zhu Y wrote the paper with support from Jin J and Lin S; all authors contributed to the general discussion.

Conflict of interest The authors declare that they have no conflict of interest.

Supplementary information Supporting data are available in the online version of the paper.

Jian Jin received her BSc (1996) and PhD degrees (2001) from Jilin University of China. She then worked as a JSPS (Japan Society for the Promotion of Science) postdoctoral fellow in the Research Center of Advanced Science and Technology at Tokyo University, Japan. From 2004 to 2009, she worked as a senior researcher at the National Institute for Materials Science, Japan, under Dr. Izumi Ichinose. In 2009, she joined Suzhou Institute of Nano-Tech and Nano-Bionics (SINANO) at the Chinese Academy of Sciences (CAS) as a group leader. Her research interests include the design of advanced filtration membranes for environmental applications.

Yuzhang Zhu received his BSc degree (2009) from Anhui University of Science and Technology and completed his PhD (2015) from the University of Chinese Academy of Sciences. He then worked as a postdoctoral fellow in Professor Jian Jin's group at SINANO, CAS. From 2017, he joined SINANO as an associate research professor. His current research interests focus on advanced membranes for nanofiltration, oil/water separation and stimuli-responsive separation.

Xiangxiu Teng received her BSc degree from Qingdao University of Science and Technology in 2016. Then, she joined Shanghai University of Science and Technology. At 2017, she started her research program under the supervision of Professor Jian Jin. Her research interest is the preparation of polyamide nanofiltration membrane for desalination.

纤维素纳米纤维薄膜支撑的具有拱形结构的高性能聚酰胺纳滤膜

滕祥秀[1,2,3,4], 方望熹[1], 梁元喆[5], 林仕弘[5], 蔺洪振[1], 刘莎莎[6], 王祯宜[1], 朱玉长[1*], 靳健[1,2*]

摘要 在废水处理、脱盐等领域, 对于具有高通量、高分离选择性的纳滤膜的需求日益增加. 通常来说, 增加纳滤膜通量的同时往往会造成膜截留率的下降. 为了能够在保证纳滤膜高的截留率的同时大幅度提升膜通量, 从而进一步突破现有纳滤膜的综合性能, 我们在本工作中报导了一种新型的高性能聚酰胺纳滤膜的制备方法. 我们利用高度水合的细菌纤维素纳米纤维薄膜作为支撑基膜, 通过在界面聚合水相单体溶液中添加NaCl, 成功制备了具有拱形结构的聚酰胺分离层纳滤膜. 这一特殊的拱形结构极大地增加了聚酰胺分离层的有效过滤面积, 使获得的纳滤膜在对Na_2SO_4保持99.1%截留率的同时, 分离通量高达42.5 L m^{-2} h^{-1} bar^{-1}, 这一性能远远优于目前已报导的聚酰胺纳滤膜.